A Micro-Insulation Concept for MEMS Applications

Rui Yao

James Blanchard
e-mail: blanchard@engr.wisc.edu

Department of Engineering Physics,
University of Wisconsin-Madison,
1500 Engineering Drive,
Madison, WI 53706

Small scale, thermally driven power sources will require appropriate insulation to achieve sufficiently high thermal conversion efficiencies. This paper presents a micro-insulation design, which was developed for a thermionic microbattery, which converts the decay heat from radioactive isotopes directly to electricity using a vacuum thermionic diode. The insulation concept, which is suitable for any small scale application, separates two planar surfaces with thin, semicircular posts, thus reducing conduction heat transfer and increasing the relative radiation heat transfer. In this case, the surfaces are silicon wafers and the columns are SU-8, a photoresist material. The experimental results indicate that this design is adequate for a practical power source concept, and they are supported by a numerical model for the effective thermal conductivity of the structure. The results show that a typical design of 20 columns/cm^2 with a 200 μm diameter and a 10 μm wall thickness has an apparent thermal conductivity on the order of 10^{-4} W/m K at a pressure of 1 Pa. System models of a thermionic power source indicate that this is sufficiently low to provide practical efficiency. [DOI: 10.1115/1.3084121]

Keywords: micro-insulation, MEMS, microscale

1 Introduction

Numerous studies have been carried out regarding technologies for providing electrical power to MEMS devices. The electrical power can be converted from various energy sources, such as chemical, solar, and radioisotopes, using a variety of conversion technologies. One example is a radioisotope powered thermionic microbattery [1,2]. The microbattery converts the radioisotope decay heat directly to electricity using a vacuum thermionic diode. At MEMS scales, due to the relatively large surface to volume ratio, the heat losses become significant. Thus a small scale thermionic device requires an appropriate thermal insulation to maintain high radioisotope source temperature and achieve high conversion efficiency. There are currently no available insulation concepts suitable for MEMS-scale applications, but there are some similar concepts used for other applications. One example is the MULTI-FOIL™ insulation developed by Thermo Electron Technologies Corporation[1] (TTC) [3,4] or the products from Actis (Limoux France). These concepts consist of evacuated layers of thin metal foils spaced by oxide particles. These structures have an apparent thermal conductivity as low as 0.001 W/m K when the cold-side temperature is 294 K [5]. The oxide particles are selected on the basis of their low thermal conductivity and compatibility with the foil chosen for the application (usually dependent on temperature). Unfortunately, the layer separation in these materials is at least a few millimeters, so it is difficult to use them at MEMS scales. An alternative is aerogel insulation, but the concept proposed here has the potential for a lower apparent thermal conductivity than a silica aerogel, which has an apparent thermal conductivity of 0.03 W/m K when the cold-side temperature is 294 K [5].

A microscale insulation concept has been proposed by Sandia National Laboratory [6]. In this approach, small conical structures, <10 μm in length, are used to separate layers of silicon, providing an analog to multifoil insulation that is suitable for MEMS applications. To date there are no published measurements of the performance of the Sandia concept. Hence, this paper presents a new concept, based on the Sandia concept, for micro-insulation suitable for MEMS and compares the measured performance to a model for heat transfer through the insulation. This micro-insulation can be designed and fabricated by semiconductor and MEMS fabrication techniques so as to be integrated easily with the other parts of a microbattery.

2 Proposed Micro-Insulation Concept

Figure 1 shows a schematic of the proposed micro-insulation concept. An array of thin-walled, half-circular columns separates the top and bottom layers, creating a gap that is evacuated to reduce gas conduction. The columns have thin walls and are fabricated from a low thermal conductivity material, such as SU-8, to minimize the solid conduction. The downward-facing surface of the top layer is coated by a low emissivity material, such as gold or silver, to reduce radiation heat transfer between the top and bottom layers. A single insulation layer fabricated in this way can also be stacked on top of another and bonded together to make a multileveled assembly. The radiation heat transfer can be reduced further by employing multiple reflecting layers.

SU-8 is a negative, epoxy-type, near-UV (350–400 nm) photoresist. It is based on the EPON® Resin SU-8 from Shell Chemical (www.shell.com/chemicals). This photoresist allows the fabrication of high aspect ratio microstructures and a broad range of thicknesses, which can be obtained in one step. Structures of up to 2 mm in height can be produced by using multiple coats. SU-8 was originally developed and patented by IBM-Watson Research Center (www.watson.ibm.com) and has been adapted for MEMS applications [7]. The thermal conductivity of this material was taken to be 0.2 W/m K [8].

This micro-insulation can be fabricated by standard lithography processes. Figure 2 illustrates the cross-sectional views of the fabrication process of a single micro-insulation. By applying appreciable pressure and temperature, the various layers of the insulation can be bonded together. Nordström et al. [9] investigated the bonding strength between SU-8 and gold. Without any adhesion promoter they found bond strengths of 4.8 ± 1.2 MPa for a 7.5 μm layer of SU-8. The value of the bond strength can be increased additionally by up to 75% using an adhesion promoter

By using OmniCoat™ and fully optimizing the processing conditions of the SU-8, Pan et al. [10] developed a silicon wafer

[1] http://www.insulation-actis.com/

Contributed by the Heat Transfer Division of ASME for publication in the JOURNAL OF HEAT TRANSFER. Manuscript received August 24, 2007; final manuscript received November 18, 2008; published online March 16, 2009. Review conducted by Roger Schmidt.

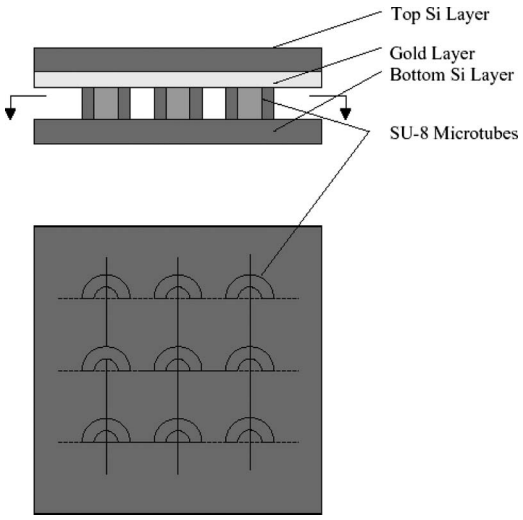

Fig. 1 Schematic of micro-insulation design (not to scale)

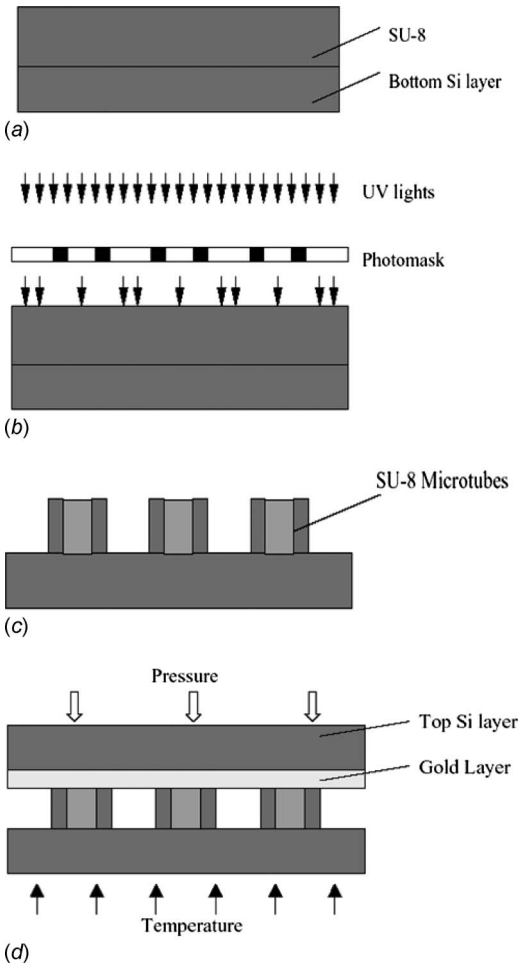

Fig. 2 (*a*) An SU-8 photoresist layer has been deposited on top of the bottom silicon substrate and soft-baked to evaporate the solvent and densify the film before exposure. (*b*) The SU-8 layer is exposed under UV lights through a photomask and baked to selectively cross-link the exposed portions of the film. (*c*) The exposed SU-8 is developed using MicroChem's SU-8 developer to form the designed structure. (*d*) The top silicon layer with gold deposited on the downward surface is placed on top of the patterned SU-8 structure.

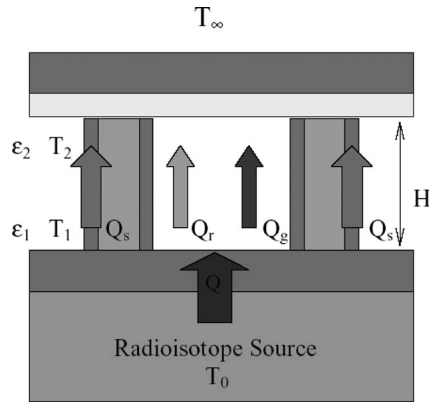

Fig. 3 Heat transfer modeling through micro-insulation. Note that Q_s represents the total heat conduction through all columns.

bonding technique and tested several patternable materials. The results indicated that SU-8 is the best material with a bonding strength of up to 20.6 MPa.

For the applications with temperatures higher than 400°C, SU-8 has to be replaced with other materials such as GaAs or SiO_2 and the fabrication processes are different from those described above.

3 Thermal Modeling

To investigate the feasibility of this concept, a computational model has been built to study the heat transfer through the layers. The schematic of the heat transfer model is shown in Fig. 3. This steady state, one-dimensional model includes several heat transfer modes, including solid conduction through the walls of the columns and gas conduction and radiation through the gap between the top and bottom layers. Free convection is not considered because the two layers are too close to allow development of convection cells even for micro-insulation at atmospheric pressure. Nonetheless, the model is most accurate at low air pressures. The Rayleigh number (the product of the Prandtl and Grashof numbers) is used to justify the decision to ignore convection [11].

In the model, Q is the total heat passing through the insulation; Q_s, Q_g, and Q_r are the heat flows through the columns, gas, and radiation, respectively; T_2 and T_∞ are the cold-side and environment temperatures and are assumed constant and identical; T_1 and T_0 are the hot-side and radioisotope source temperatures, respectively, and are assumed to be identical; ε_1 and ε_2 are the emissivities of the top and bottom layers, respectively; and H is the height of the columns. The model assumes that there are no heat losses laterally, which means all heat fluxes are parallel to the axial direction of the columns and that all surfaces are gray surfaces so that their emissivities are independent of the wavelength of the radiation.

For the problems involving combined radiation and conduction, a simple approach is to assume that both heat transfer modes are uncoupled and the desired temperatures and heat fluxes can be found by adding separate solutions. Unfortunately, uncoupled problems are not as common as coupled problems, especially when the total energy flux is specified, so the entire problem typically must be treated simultaneously because of the nonlinear coupling of the unknown temperatures [12].

The energy balance equation is

$$Q = Q_S + Q_r + Q_g = Q \cdot (\eta_S + \eta_r + \eta_g) \tag{1}$$

where η_S, η_r, and η_g represent the fractions of total heat flows by solid conduction, radiation, and gas conduction, respectively, and Q is the total heat flow.

The heat flow by conduction through the columns is given by

$$Q_s = Q \cdot \eta_S = \frac{k_s A_s}{H}(T_1 - T_2) \tag{2}$$

where k_s is the thermal conductivity of the column material and A_s is the total cross-sectional area of the columns.

The heat flow by radiation from the bottom layer to the top layer is given by

$$Q_r = Q \cdot \eta_r = \frac{\sigma \cdot A_r \cdot (T_1^4 - T_2^4)}{\left(\frac{1}{\varepsilon_1} + \frac{1}{\varepsilon_2} - 1\right)} \tag{3}$$

where σ is the Stefan–Boltzmann constant, ε_1 and ε_2 are the emissivities of the top and bottom layer surfaces, and A_r is the total radiation cross-sectional area.

Heat conduction in gases is normally divided into four separate molecular regimes: free-molecule (Kn$>$10), transition (10$>$Kn$>$0.1), temperature-jump (slip) (0.1$>$Kn$>$0.01), and continuum (Kn$<$0.01), where Kn is the Knudsen number (Kn$=\lambda/H$, where λ is the mean free path of the gaseous molecules and H is the characteristic length of the gas layer). Based on the Maxwell–Boltzmann distribution of velocities, the mean free path of gaseous molecules in an infinite space is given by

$$\lambda = \frac{1}{\sqrt{2}\pi \cdot d^2 n} = \frac{k_B T}{\sqrt{2}\pi \cdot d^2 P} \tag{4}$$

where d is the diameter of air molecules, n is the number of molecules per unit volume, k_B is the Boltzmann constant, T is the temperature, and P is the pressure. For example, assuming an air molecule diameter of 3 Å at a temperature of 400 K and pressure of 1 Pa, we find $\lambda = 13.8$ mm. Since the mean free path is much larger than the characteristic length of the micro-insulation, the effective mean free path is constrained by the height of the columns.

The heat flux through the gas is given by [13]

$$Q''_{\mathrm{FM}} = \frac{1}{2}(\gamma+1)c_V \frac{P}{\sqrt{2\pi RT}} \cdot \frac{\alpha_1 \alpha_2}{\alpha_1 + \alpha_2 - \alpha_1 \alpha_2}(T_1 - T_2) \tag{5}$$

and the gas thermal conductivity is

$$k_{\mathrm{gas}} = \frac{1}{2}(\gamma+1)c_v \frac{P}{\sqrt{2\pi RT}} H \tag{6}$$

where γ is the ratio of the heat capacity at constant pressure to that at constant volume, c_v is the heat capacity at constant volume, T_1 and T_2 are the temperatures at the two boundaries, T is the mean temperature of T_1 and T_2, R is the universal gas constant, P is the gas pressure at T, and α_1 and α_2 are the accommodation coefficients of the gaseous molecules on the two boundaries. The accommodation coefficient is a measure of the efficiency of thermal energy interchange that occurs when a gas molecule collides with the surface. It varies between 1 (complete accommodation and diffuse re-emission) and 0 (specular re-emission). Its exact value depends on the kind of gas molecule, the surface temperature, and, most importantly, the surface condition.

When the vacuum is from approximately 1 Torr to atmospheric pressure (760 Torr), the heat transfer falls into the transition regime (10$>$Kn$>$0.1). Gas conduction in this regime is rather complicated. For practical calculations, the following simple interpolation formula is suggested by Sherman [14]:

$$\frac{Q''}{Q''_{\mathrm{FM}}} = \frac{1}{1 + \frac{Q''_{\mathrm{FM}}}{Q''_C}} \tag{7}$$

where Q'' is the transition heat flux, Q''_{FM} is the free-molecule heat flux given in Eq. (5), and Q''_C is the continuum heat flux. For a plane layer, Q''_C can be written from the simple kinetic theory as

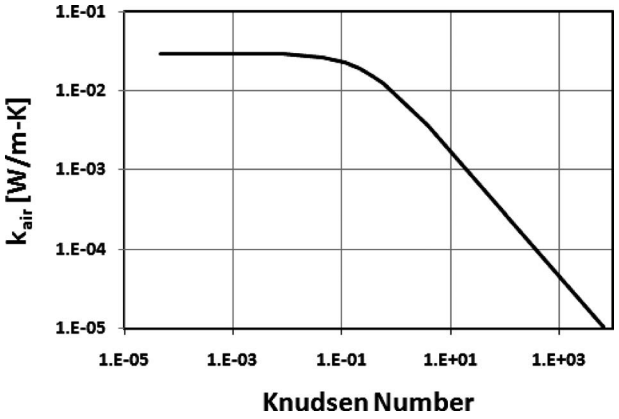

Fig. 4 Thermal conductivity of air at 400 K as a function of Knudsen number

$$Q''_C = \frac{k_{\mathrm{gas},C}(T_1 - T_2)}{H} = \frac{9\gamma - 5}{4}\mu \cdot c_v \frac{T_1 - T_2}{H} \tag{8}$$

where c_v is the constant volume specific heat and μ is the dynamic viscosity.

Figure 4 shows the air thermal conductivity as a function of Knudsen number for a given air gap (therefore also a function of pressure) at 400 K. Although the free-molecule conduction is the most efficient conduction mode, the air thermal conductivity decreases linearly with pressure because of the decreasing number of air molecules involved. In the transition regime, energy is transported less efficiently due to the collisions between air molecules, but the higher molecule density makes the thermal conductivities increase. In the continuum regime, the gas particles and mean free path are directly and indirectly proportional to the gas pressure and the gas thermal conductivity is independent of pressure. From Fig. 4 we can also estimate that for this micro-insulation design, to obtain a thermal conductivity on the order of 10^{-4} W/m K, the Knudsen number should be at least 500.

In the micro-insulation design described in this paper, the two layers are so close that the gas conduction between them is in the free-molecule regime. Thus the heat flow by conduction through the gas is

$$Q_g = Q \cdot \eta_g = k_{\mathrm{gas}} \cdot A_g \cdot (T_1 - T_2) \tag{9}$$

where A_g is the gas conduction cross-sectional area, assumed to be identical to A_r, and k_{gas} is the gas thermal conductivity at the mean temperature of T_1 and T_2.

By solving Eqs. (1)–(9), the thermal transmittance of the micro-insulation can be obtained as

$$C = \frac{Q}{(T_1 - T_2)A} \tag{10}$$

where A is the cross-sectional area of the top and bottom layers.

The apparent thermal conductivity of the micro-insulation, which is convenient for comparison to conduction through suitable solid materials, is defined as

$$k_{\mathrm{app}} = C \cdot H \tag{11}$$

The conceptual design parameters used in this model are given in Table 1.

4 Experimental Results

To test the ability of the proposed micro-insulation to provide the characteristics needed for a small scale application, a representative sample was fabricated for testing. This sample consisted of two silicon wafers (10 cm in diameter) separated by semicircular, SU-8 columns with a wall thickness of 10 μm and height of 45 μm. The column density is 20 columns/cm^2. The apparatus

Table 1 Design parameters of a typical micro-insulation concept

Parameters	Values
Top and bottom layers' cross-sectional area, A	1×1 cm^2
Heights of columns, H	10 μm
Vacuum between the two layers, P	1 Pa
Diameter of columns (outer), D	200 μm
Wall thickness of columns, δ	10 μm
Cold-side temperature, T_2	300 K
Total heat applied on the micro-insulation, Q	1 W
Top and bottom layers' surface emissivities, ε_1 and ε_2	0.05 and 0.5
Thermal conductivity of SU-8, k_s	0.2 W/m K
Top and bottom layers' accommodation coefficients, α_1 and α_2	0.9 and 0.9
No. of columns	20

for measuring the micro-insulation's apparent thermal conductivity is shown schematically in Fig. 5. The apparatus is intended to establish one-dimensional heat flow through a micro-insulation specimen sandwiched by two parallel heat flux transducers. An infrared lamp, producing 3 W, was used to generate an appropriate input heat flux from one side. The entire experiment was carried out in a small vacuum chamber. This approach eliminated the need to seal the insulation itself, so the feasibility of sealing the insulation for practical applications is an open question that requires further research. The ratio of the sample diameter to the entire insulation thickness is chosen to be 100 in order to reduce the side losses.

Two BF-02 heat flux transducers from Vatell Corporation (www.vatell.com) are used to measure the heat flux and temperature at both sides of the micro-insulation. The heat flux transducer is also associated with a T type thermocouple. The thermal conductivity of the BF-02 is 0.25 W/m K and the thickness is 0.25 mm, with several thermocouples through the thickness. Hence, so the temperature drop through the surface thermocouple is small and can be neglected. Similarly, the sensor is attached to the insulation surface with a thin (0.127 mm), high conductivity tape, providing good thermal contact with negligible impact on the measured surface temperature.

By measuring the hot-side and cold-side heat fluxes q_h'' and q_c'', the hot and cold temperatures T_h and T_c, and the average height of the columns H, the apparent thermal conductivity can be obtained by

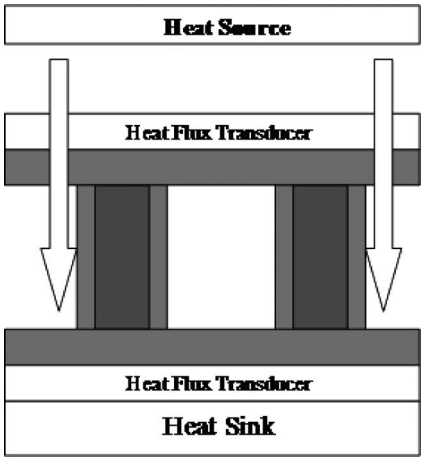

Fig. 5 The apparatus for thermal conductivity measurement

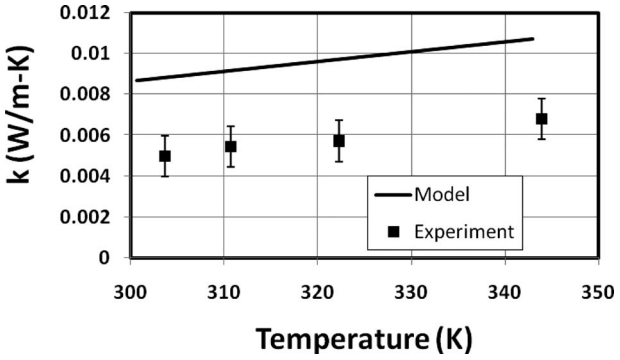

Fig. 6 Apparent thermal conductivity of micro-insulation at atmospheric pressure as a function of hot-side temperature

$$k_{\exp}=\frac{(q_h''+q_c'')H}{2(T_h-T_c)} \tag{12}$$

The average of the hot-side and cold-side heat fluxes has been used here because it provides a conservative estimate of the apparent thermal conductivity of the micro-insulation. The two heat fluxes differ because some heat entering the hot-side sensor conducts laterally and radiates away from the top surface of the hot-side wafer, thus reducing the heat transferred through the micro-insulation. Hence, the cold-side sensor provides a better estimate of the heat flux transporting through the insulation, but there is some chance that lateral losses are also an issue. Hence, the average is used to be conservative.

Figure 6 shows that at atmospheric pressure, the measured apparent thermal conductivities of the micro-insulation are lower than the theoretical values. The reason for this disagreement is that the heat losses from the edge of the micro-insulation and from the top silicon wafer are not taken into account in the model. When the pressure is reduced, these losses are significantly reduced and the agreement between the experiment and the model is improved. This is shown in Fig. 7, which shows the comparison at a pressure of 6.5 Pa (50 mTorr). Figure 8 shows a comparison of the measured and theoretical apparent thermal conductivities at pressures ranging from 2 Pa to 120 Pa. In all cases, the cold-side temperature was approximately 50°C and the hot-side temperature varied according to the apparent thermal conductivity.

5 Discussion

To further assess the ability of the proposed micro-insulation to provide adequate performance in a MEMS application, parametric studies have been carried out to assess the impact in design varia-

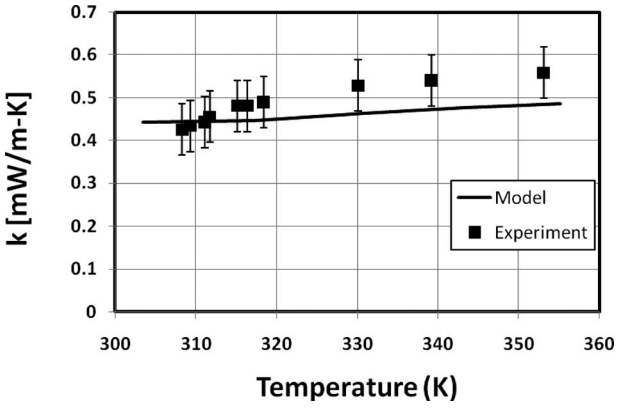

Fig. 7 Apparent thermal conductivity of micro-insulation at 6.5 Pa as a function of hot-side temperature

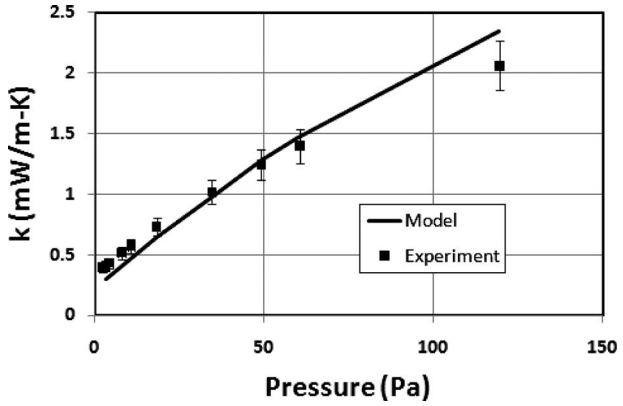

Fig. 8 Apparent thermal conductivity as a function of pressure. The cold-side temperature began at room temperature and reached a steady state temperature of approximately 50°C before the apparent thermal conductivity was determined.

tions around the nominal specifications used in the experiments described in Sec. 4. Figure 9 shows the variation of the apparent conductivity and hot-side temperature as a function of pressure, demonstrating that below pressures on the order of a few pascals the micro-insulation can achieve apparent conductivities of approximately 1.5×10^{-4} W/m K. This indicates that such a design can achieve an apparent thermal conductivity, which is two orders of magnitude below a typical silica aerogel and on the same order of commercial MULTI-FOIL insulation. From Fig. 4 we conclude that in the transition regime, the air thermal conductivity decreases very slowly with vacuum, which results in a situation in which gas conduction dominates the heat transfer when the pressure is higher than 5 Pa (Fig. 10). Furthermore, for a certain design of this micro-insulation, there exists a pressure limit, beyond which lowering the pressure will not improve the heat transfer performance significantly.

At higher vacuum (pressures less than 1 Pa), conduction through the column wall becomes important. Decreasing the number or wall thickness of the columns would reduce the heat conduction cross-sectional area between the top and bottom layers. Thus a lower thermal conductivity can be obtained (Fig. 11). On the other hand, very thin wall thicknesses and inadequate numbers of columns can result in a mechanical instability of the micro-insulation structure, so there is a limit to the allowed spacing between tubes.

A low emissivity coating on the downward surface of the top layer can reduce radiation loss through the micro-insulation. Figure 12 shows that compared with a silicon layer without a coating (assuming emissivity of 0.5), a gold coating (emissivity of 0.05) can reduce the apparent thermal conductivity by about 40%. A gold coating on the upward surface of the bottom layer can reduce the radiation loss further.

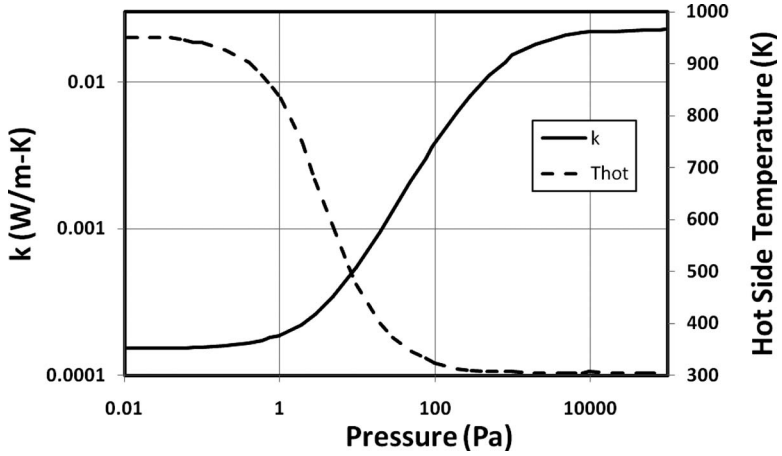

Fig. 9 The apparent thermal conductivity and hot-side temperature as a function of pressure

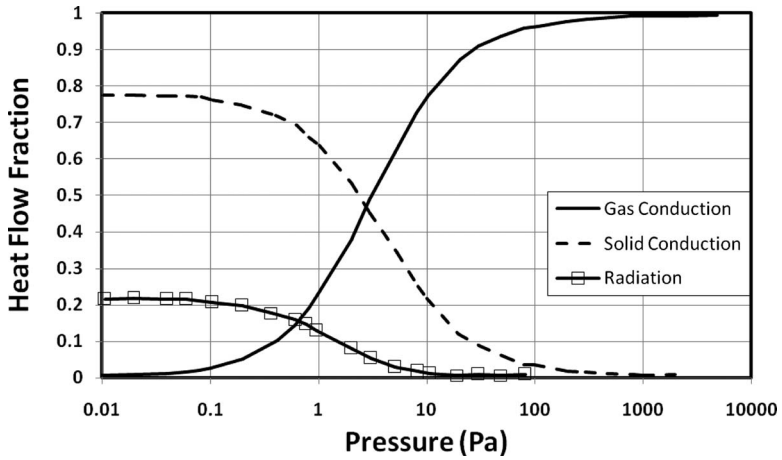

Fig. 10 The fraction of heat flow contribution from radiation, gas conduction, or solid conduction as a function of pressure

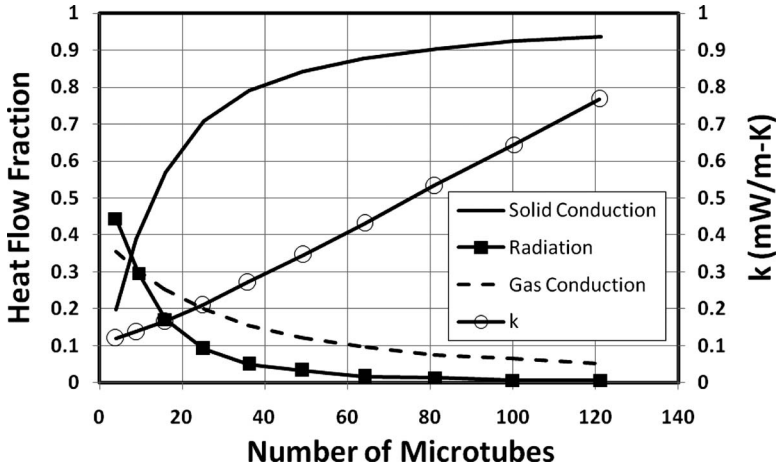

Fig. 11 The apparent thermal conductivity and heat flow contributions as a function of the number of columns at a pressure of 1 Pa

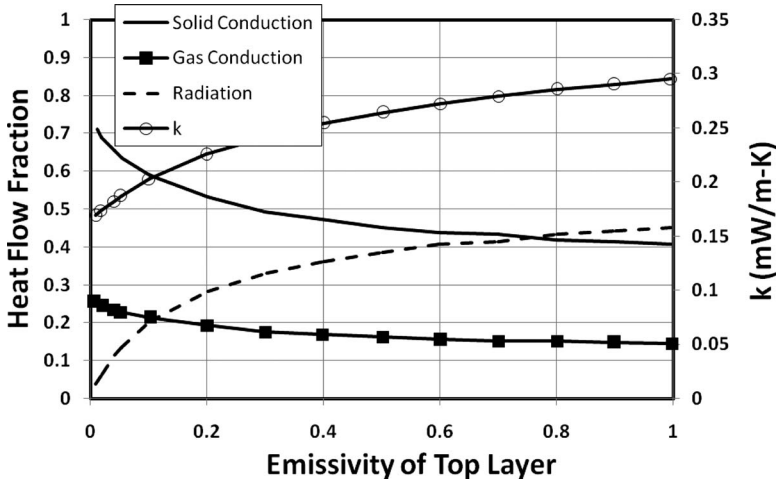

Fig. 12 The apparent thermal conductivity and heat flow contributions as a function of the top layer emissivity at a pressure of 1 Pa

6 Conclusions

This paper has demonstrated that effective micro-insulation can be fabricated using silicon layers separated by SU-8 columns. At pressures below about 1 Pa, gas conduction is minimized and the heat transfer is dominated by solid conduction through the columns and radiation. For a design that consists of 20 columns/cm^2 with a 200 μm diameter and a 10 μm wall thickness, experiments and modeling indicate an apparent thermal conductivity on the order of 10^{-4} W/m K at a device pressure of 1 Pa. Better results can be achieved by decreasing the areal density of the columns, further reducing the pressure (though this has minimal return below 1 Pa), decreasing the thermal conductivity of the column material, or reducing the emissivity of the surfaces of the micro-insulation. These results indicate the feasibility of using this micro-insulation concept in a practical, thermally driven power source. To truly demonstrate viability, the design must include a concept for sealing the device without creating a thermal shunt. This requires further work.

Acknowledgment

This work was supported by the Department of Energy, through the NEER program.

Nomenclature

A = heat transfer cross-sectional area, m^2
C = thermal transmittance, W/m^2 K
c_v = constant volume specific heat, J/kg K
d = diameter of air molecules, m
H = height of columns, m
k = thermal conductivity, W/m K
k_B = Boltzmann constant, 1.38×10^{-23} J/K
Kn = Knudsen number
n = number of molecules per unit volume
P = pressure between the two silicon layers, Pa
Q = heat flow, W
R = universal gas constant, 8.31 J/mol K
T = temperature, K
α = accommodation coefficient
γ = the ratio of the heat capacity at constant pressure to that at constant volume
δ = wall thickness of columns, m
ε = emissivity
η = fraction of heat flows through the micro-insulation
λ = mean free path, m
μ = dynamic viscosity, kg/s m

σ = Stefan–Boltzmann constant, 5.67×10^{-8} W/m^2 K^4
σ_{cr} = local buckling critical stress, Pa

Subscripts

1 = top (hot) layer
2 = bottom (cold) layer
c = continuum conduction
FM = free-molecule conduction
g = gaseous phase conduction
r = radiation heat transfer
s = solid phase conduction

References

[1] Hernqvist, K. G., 1960, "Thermionic Power Conversion and Its Possibilities in the Nuclear Field," *Direct Conversion of Heat to Electricity*, J. Kaye and J. A. Welsh, eds., Wiley, New York, Chap. 9.
[2] King, D. B., Sadwick, L. P., and Wernsman, B. R., 2001, "Microminiature Thermionic Converters," U.S. Patent No. 6,294,858.
[3] Dunlay, J. B., 1967, "The Development of Foil Thermal Insulation of High Temperature Heat Sources," *Proceedings of the Second Intersociety Energy Conversion Engineering Conference*, ASME, New York.
[4] Paquin, M. L., 1969, "The MULTI-FOIL Thermal Insulation Development Program," *Proceedings of the Fourth Intersociety Energy Conversion Engineering Conference*, ASCE, New York.
[5] Kreith, F., 2000, *The CRC Handbook of Thermal Engineering*, CRC, Boca Raton, FL, pp. 4–194.
[6] Marshall, A., Kravitz, S., Tigges, C., and Vawter, G., 2004, "Methods for Fabricating a Micro Heat Barrier," U.S. Patent No. 6673254.
[7] Lorenz, H., Despont, M., Fahrni, N., LaBianca, N., Prenaud, P., and Vettiger, P., 1997, "SU-8: A Low-Cost Negative Resist for MEMS," J. Micromech. Microeng., **7**, pp. 121–124.
[8] Chang, S., Warren, J., Hong, D., and Chiang, F., 2002, "Testing Mechanical Properties of EPON SU-8 With SIEM," 2002 SEM Annual Conference and Exposition on Experimental and Applied Mechanics, Milwaukee, WI, p. 2002.
[9] Nordström, M., Johansson, A., Nogueron, S., Clausen, B., Calleja, M., and Boisen, A., 2005, "Investigation of the Bond Strength Between the Photo-Sensitive Polymer SU-8 and Gold," Microelectron. Eng., **78–79**, pp. 152–157.
[10] Pan, C.-T., Yang, H., Shen, S.-C., Chou, M.-C., and Chou, H.-P., 2002, "A Low-Temperature Wafer Bonding Technique Using Patternable Materials," J. Micromech. Microeng., **12**, pp. 611–615.
[11] Incropera, F. P., and Dewitt, D. P., 2002, *Fundamentals of Heat and Mass Transfer*, Wiley, New York.
[12] Siegel, R., and Howell, J. R., 1992, *Thermal Radiation Heat Transfer*, Hemisphere, New York.
[13] Devienne, F. M., 2002, "Low Density Heat Transfer," *Advances in Heat Transfer*, Vol. 2, Academic, New York.
[14] Sherman, F. S., 1963, "A Survey of Experimental Results and Methods for the Transition Regime of Rarefied Gas Dynamics," *Rarefied Gas Dynamics*, Vol. II, J. A. Lauermann, ed., Academic, New York, pp. 228–260.